NASA TECHNICAL NOTE

EFFECT OF REYNOLDS NUMBER ON OVERALL PERFORMANCE OF A 6-INCH RADIAL BLADED CENTRIFUGAL COMPRESSOR

by Laurence J. Heidelberg, Calvin L. Ball,
and Carl Weigel

Lewis Research Center
Cleveland, Ohio

NATIONAL AERONAUTICS AND SPACE ADMINISTRATION • WASHINGTON, D. C. • APRIL 1970

1. Report No. NASA TN D-5761	2. Government Accession No.	3. Recipient's Catalog No.
4. Title and Subtitle EFFECT OF REYNOLDS NUMBER ON OVERALL PERFORMANCE OF A 6-INCH RADIAL BLADED CENTRIFUGAL COMPRESSOR		5. Report Date April 1970
		6. Performing Organization Code
7. Author(s) Laurence J. Heidelberg, Calvin L. Ball, and Carl Weigel		8. Performing Organization Report No. E-4879
9. Performing Organization Name and Address Lewis Research Center National Aeronautics and Space Administration Cleveland, Ohio 44135		10. Work Unit No. 120-27
		11. Contract or Grant No.
		13. Type of Report and Period Covered Technical Note
12. Sponsoring Agency Name and Address National Aeronautics and Space Administration Washington, D.C. 20546		
		14. Sponsoring Agency Code

15. Supplementary Notes

16. Abstract

Overall performance is presented over a range of compressor inlet pressures from a nominal 1.5 to 8.6 psia (1.0×10^4 to 5.9×10^4 N/m^2 abs) and corresponding Reynolds number range of 0.32×10^6 to 1.8×10^6. As inlet pressure and thus Reynolds number was decreased, a progressive degradation in efficiency along with a lowering of the surge and maximum flow points was observed. These changes in performance are explained in terms of changing viscous losses and changing effective flow areas with Reynolds number. A comparison between the data and the commonly used 0.2 power of Reynolds number relation to loss is made.

17. Key Words (Suggested by Author(s)) Centrifugal compressor Reynolds number Space power Brayton cycle Viscous losses Turbomachinery		18. Distribution Statement Unclassified - unlimited		
19. Security Classif. (of this report) Unclassified	20. Security Classif. (of this page) Unclassified		21. No. of Pages 25	22. Price* $3.00

EFFECT OF REYNOLDS NUMBER ON OVERALL PERFORMANCE OF A
6-INCH RADIAL BLADED CENTRIFUGAL COMPRESSOR

by Laurence J. Heidelberg, Calvin L. Ball, and Carl Weigel

Lewis Research Center

SUMMARY

A 6-inch (15.24-cm) radial-bladed centrifugal compressor designed for a 10-kilowatt Brayton cycle power system was tested in air over a range of compressor inlet pressure from a nominal 1.5 to 8.6 psia (1.0×10^4 to 5.9×10^4 N/m^2). The corresponding Reynolds number range is from 0.32×10^6 to 1.8×10^6. The effect of compressor inlet pressure and thus Reynolds number on compressor efficiency, work factor, pressure ratio, and flow range is shown. A progressive degradation in efficiency along with a lowering of the surge and maximum flow points with decreasing Reynolds number was observed. These changes in performance are explained in terms of changing viscous losses and changing effective flow areas with Reynolds number. A comparison between the data and the commonly used 0.2 power of Reynolds number relation to loss is made.

INTRODUCTION

One of the methods which shows promise for generating electrical power in space is the closed Brayton cycle system. As space missions vary the required amounts of electrical power will vary. Because of the time and cost involved in developing the rotating machinery for the Brayton cycle system, it is desirable to take a basic set of hardware developed for a nominal power level and use it for a range of power outputs. This can be accomplished by varying the power developed by the turbine by varying the mass flow rate passing through the turbine and thus that circulating within the system. One method of adjusting the mass flow rate is to vary the density of the circulating gas by adjusting the system pressure level. This method has the potential of providing a wide range of power adjustment. However, it results in a change in Reynolds number at which the turbomachinery must perform. Changes in compressor efficiency can result from changes in Reynolds number. Small changes in compressor efficiency have a pronounced effect on the size and weight of the heat-transfer components.

A limited amount of Reynolds number data exists for small compressors suitable for Brayton cycle space power systems. To better establish the change in performance with Reynolds number, an experimental program was initiated using a small radial bladed centrifugal compressor suitable for space power applications. The compressor was designed for use in argon gas which is one of the working fluids considered for the Brayton cycle space power system (refs. 1 and 2). The compressor design and fabrication (ref. 3) was accomplished by contract to AiResearch Manufacturing Company, Division of the Garrett Corporation, Phoenix, Arizona. The overall performance in argon was reported in reference 4.

In this investigation the testing was done in air. The Reynolds number was varied from 0.32×10^6 to 1.8×10^6 by varying the compressor inlet pressure from nominal values of 1.5 to 8.6 psia (1.0×10^4 to 5.9×10^4 N/m^2). All performance data reported herein were obtained in tests at the Lewis Research Center.

SYMBOLS

c_p specific heat at constant pressure, Btu/(lb)(^{O}R); J/(kg)(K)

D diameter, ft; m

f_{cw} compressor work factor, $gJc_p(T_6 - T_1)/U_{t3}^2$

f_s slip factor, $V_{ut3}/U_{t3} = gJc_p \Delta T_{vd}/U_{t3}^2$

f_w windage factor, $gJc_p \Delta T_w/U_{t3}^2$

g gravitational acceleration, 32.17 ft/sec^2; 9.807 m/sec^2

H ideal head rise, ft; m

J mechanical equivalent of heat, 778.16 ft-lb/Btu; 0.999 N-m/J

N_s specific speed, $\text{rpm}\sqrt{Q}/60(gH)^{3/4}$

n exponent for Reynolds number - loss correlation

P total (stagnation) pressure, psia (N/m^2)

p static pressure, psia; N/m^2

Q volume flow rate, ft^3/sec; m^3/sec

R gas constant, ft-lb/(lb)(^{O}R); (N-m)/(kg)(K)

Re Reynolds number, $\rho_1 U_{t3} D_{t3}/\mu_1$

rpm impeller rotational speed, rpm

T	total (stagnation) temperature, ^{O}R; K
ΔT_{vd}	gas temperature rise associated with vector diagrams, ^{O}R; K
ΔT_{w}	gas temperature rise associated with windage, ^{O}R; K
U	impeller wheel speed, ft/sec; m/sec
V	absolute gas velocity, ft/sec; m/sec
W	weight (mass) flow rate, lb/sec; kg/sec
γ	ratio of specific heat at constant pressure to specific heat at constant volume, c_p/c_v
δ	ratio of compressor inlet total pressure to U. S. standard sea level pressure, $P_1/14.7$ psia; $(P_1/101.35{\times}10^3 \text{ N/m}^2)$
η	adiabatic temperature rise efficiency, $T_1\left[(P_6/P_1)(P_6/P_1)^{(\gamma-1)/\gamma}-1\right]\Big/(T_6 - T_1)$
θ	ratio of compressor inlet total temperature to U. S. standard sea level temperature, $T_1/518.7^{O}$ R $(T_1/288.17$ K)
φ	inlet flow coefficient, $(V_m/U)_2$

Subscripts:

m	meridional component
t	tip
u	tangential component
1	station in inlet pipe 5 in. (12.7 cm) upstream of compressor inlet flange (fig. 4)
2	station at impeller inlet (fig. 4)
3	station at impeller outlet (fig. 4)
4	station at diffuser blade inlet (fig. 4)
5	station at diffuser blade outlet (fig. 4)
6	station in exit pipe 3 in. (7.62 cm) downstream of compressor scroll exit flange (fig. 4)

Superscript:

'	relative to impeller

COMPRESSOR DESIGN

The compressor was designed to fit a specific closed Brayton cycle space power system with argon as the working fluid. The values of the compressor design parameters for argon as the working fluid and the equivalent values for standard inlet conditions are given in table I.

The data presented in this report were obtained with air as the working fluid. The values of the compressor design parameters with air as the working fluid and the equivalent values for standard inlet conditions are given in table II. The method used to obtain the design values for air as the working fluid is presented in appendix A. A comparison between air and argon performance based on this correlation is also presented in appendix A.

TABLE I. - VALUES OF COMPRESSOR DESIGN PARAMETERS

(WORKING FLUID - ARGON)

Compressor design parameters	Based on design inlet pressure and temperature	Based on standard inlet pressure and temperature
Inlet total pressure, P_1, psia (N/m^2)	6 (41.36×10^3)	14.7 (101.35×10^3)
Inlet total temperature, T_1, $^\circ$R (K)	536 (297.78)	518.7 (288.17)
Weight flow rate, W, lb/sec (kg/sec)	0.611 (0.278)	1.52 (0.69)
Compressor total pressure ratio, P_6/P_1	2.38	[a]2.38
Compressor total temperature ratio, T_6/T_1	1.525	[a]1.525
Compressor efficiency, η_{1-6}	0.798	[a]0.798
Impeller total pressure ratio, P_3/P_1	2.62	[a]2.62
Impeller efficiency, η_{1-3}	0.896	[a]0.896
Rotative speed, rpm	38 500	37 900
Impeller tip speed, U_{t3}, ft/sec (m/sec)	1004 (306)	989 (301.5)
Impeller slip factor, f_s	0.830	[a]0.830
Impeller windage factor, f_w	0.039	[a]0.039
Compressor work factor, f_{cw}	0.869	[a]0.869
Specific speed, N_s	0.1057	0.1057
Reynolds number, Re	1.36×10^6	3.42×10^6

[a]These values are approximate and in actuality will differ from design as a result of the difference in Reynolds number.

TABLE II. – VALUES OF COMPRESSOR DESIGN PARAMETERS

(WORKING FLUID - AIR)

Compressor design parameters	Based on design inlet pressure and temperature	Based on standard inlet pressure and temperature
Inlet total pressure, P_1, psia (N/m^2)	6.41 (44.2×10^3)	14.7 (101.35×10^3)
Inlet total temperature, T_1, °R (K)	536 (297.78)	518.7 (288.17)
Weight flow rate, W, lb/sec (kg/sec)	0.497 (0.225)	1.155 (0.524)
Compressor total pressure ratio, P_6/P_1	2.09	[a]2.09
Compressor total temperature ratio, T_6/T_1	1.30	[a]1.30
Compressor efficiency, η_{1-6}	0.798	[a]0.798
Impeller total pressure ratio, P_3/P_1	2.27	[a]2.27
Impeller efficiency, η_{1-3}	0.896	[a]0.896
Rotative speed, rpm	40 300	39 700
Impeller tip speed, U_{t3}, ft/sec (m/sec)	1051 (320.3)	1035 (315.5)
Impeller slip factor, f_s	0.830	[a]0.830
Impeller windage factor, f_w	0.039	[a]0.039
Compressor work factor, f_{cw}	0.869	[a]0.869
Specific speed, N_s	0.1057	0.1057
Reynolds number, Re	1.36×10^6	3.25×10^6

[a]These values are approximate and in actuality will differ from design as a result of the difference in Reynolds number.

Impeller Design

Fifteen blades were chosen for the impeller. The impeller exit diameter required to satisfy the compressor design values was calculated to be 5.976 inches (15.179 cm). The impeller exit blade height was set at 0.217 inch (0.551 cm). Impeller inlet dimensions were selected based on the desired inlet flow conditions and their relation to the exit diameter for good impeller efficiencies. The impeller inlet tip diameter was set at 3.528 inches (8.961 cm) and the hub diameter at 1.858 inches (4.719 cm). Design velocity diagrams for the impeller inlet and outlet with air as the working fluid are shown in figure 1. A more complete description of design considerations and procedures for this impeller, diffuser, and scroll is given in references 3 and 4.

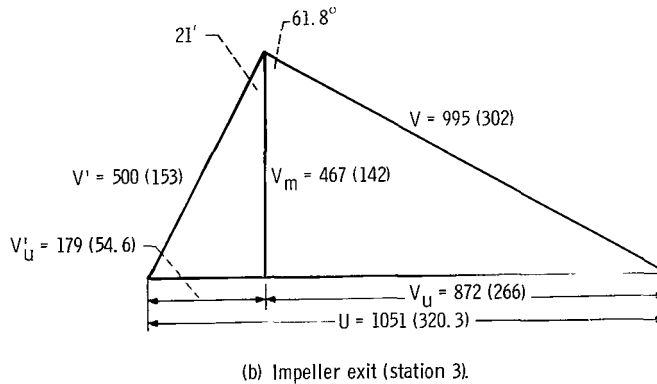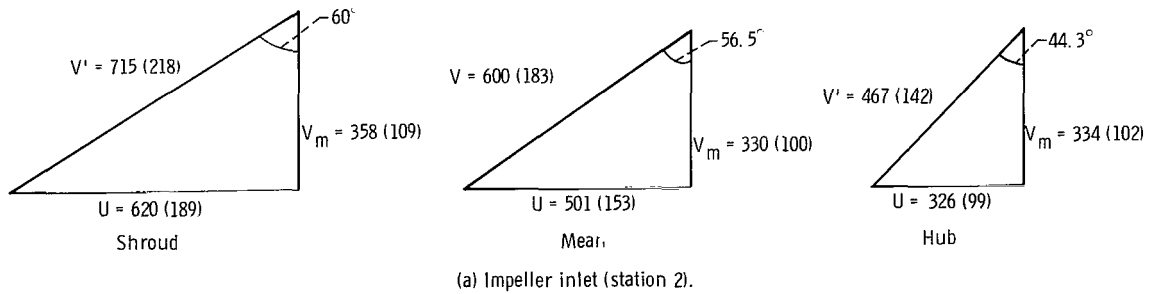(a) Impeller inlet (station 2).

(b) Impeller exit (station 3).

Figure 1. - Impeller design velocity diagrams. (All dimensions in feet per second (m/sec) unless indicated otherwise.)

Diffuser and Scroll Design

A short vaneless diffuser, about 0. 10 inch (0. 254 cm) long in the radial-direction was used between the impeller exit and diffuser vane inlet. The diffuser vane shapes were designed to give a gradual deceleration on both suction and pressure surfaces.

The scroll was designed with essentially circular cross sections which were located to blend with the diffuser flow passage. The circumferential variation in cross sectional area was selected based on satisfying the condition of constant angular momentum and continuity of mass flow. The design Mach number at the compressor exit flange was 0. 16. Design velocity diagrams at diffuser vane inlet and exit for air are shown in figure 2.

Preliminary experimental tests conducted by the contractor using the design compressor configuration resulted in lower than design weight flow. An adjustment to the diffuser vane angle was made in order to more closely approach the design pressure ratio at design weight flow. The final compressor configuration used diffuser vanes having an angle setting 3° less than the design angle as measured from the radial direction.

$V_m \approx 417\ (127)$ 63.35' $V \approx 929\ (284)$

$V_u \approx 831\ (253)$
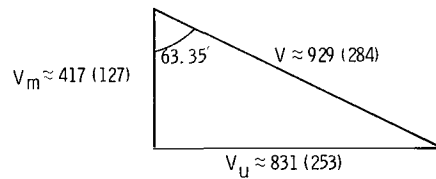
(a) Diffuser inlet diagram (station 4) based on effec-
tive flow area which includes vane leading edge
blockage.

$V_m \approx 251\ (76.5)$ $63.35°$ $V \approx 560\ (170)$

$V_u \approx 500\ (153)$
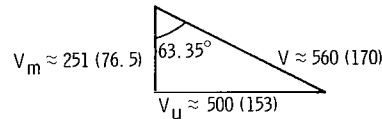
(b) Diffuser exit diagram (station 5) based on
core flow conditions.

Figure 2. - Diffuser design velocity diagrams. (All
dimensions in feet per second (m/sec) unless other-
wise indicated.)

APPARATUS AND PROCEDURE

The test apparatus, test facility instrumentation, and test procedure is basically
the same as that presented in reference 4 with the exception of air being employed as
the working fluid instead of argon. These sections are essentially repeated herein for
quick reference.

Test Apparatus

The compressor package consisted of the aerodynamic hardware, bearing-seal
shaft assembly, and stand. A cutaway view of the compressor package is shown in fig-
ure 3. The locations of instrumentation and calculation stations are shown in the figure.
The compressor impeller was cantilever mounted on a shaft supported by two angular
contact bearings. Carbon face seals outboard of each bearing were used to prevent
bearing oil leakage. The static impeller clearance between the shroud and blade tip at
impeller discharge was set at 0.010 inch (0.0254 cm).

The impeller in this investigation was machined from a titanium forging and is shown
in figure 4. This figure also shows the vaned diffuser located downstream of the impeller.
The vaned diffuser has 23 blades which are integral with the vaned diffuser blade ring
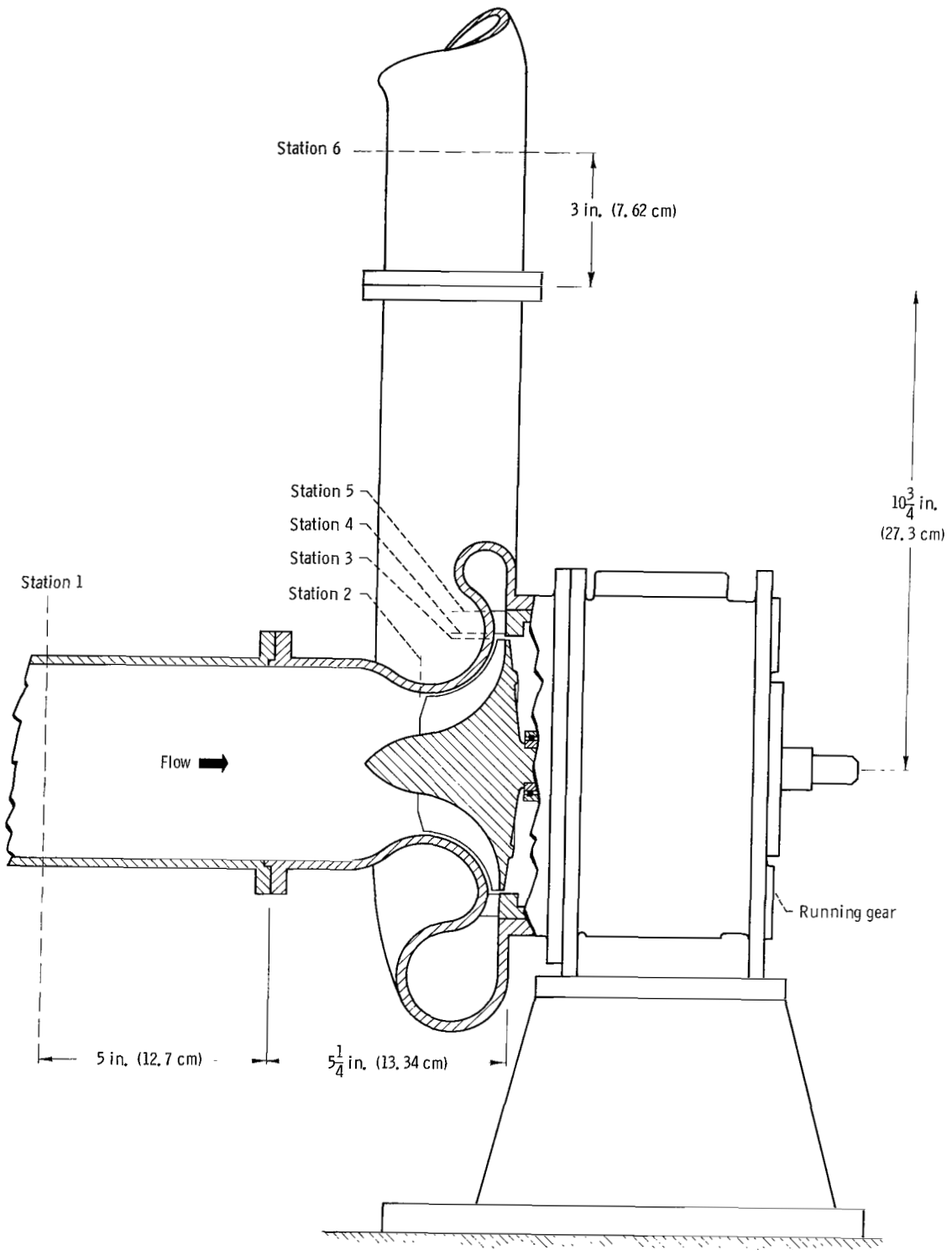
Figure 3. - Compressor package.

CD-9754-01
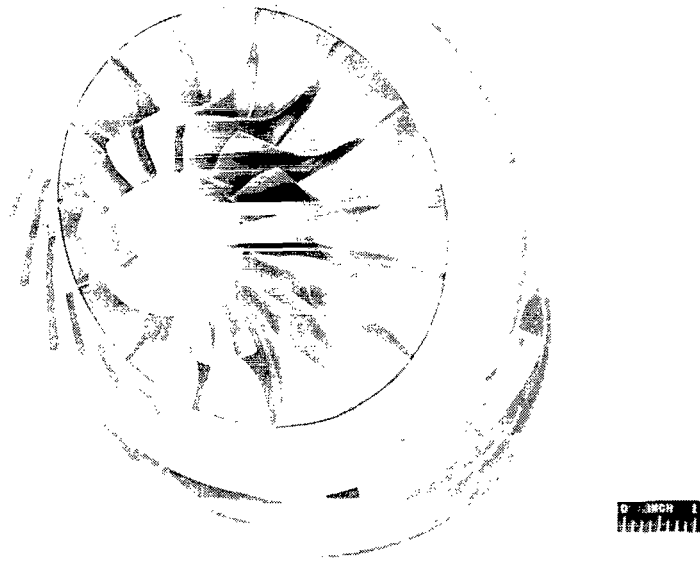
C-66-4626

Figure 4. - Impeller and vaned diffuser.

and were machined from 347 stainless-steel material. The diffuser vane tips were con-
toured to fit the machined aluminum casting that comprised the compressor scroll,
impeller shroud, and inlet.

The compressor drive unit consisted of a single-stage axial-flow air turbine. The
turbine was connected to the compressor package by a high-speed coupling. Turbine
speed was controlled by a remotely operated electropneumatic valve.

Test Facility

The test facility used in this investigation is an open-loop system with inlet pressure
control. This facility is shown schematically in figure 5. In this investigation laboratory
dry air was supplied to the compressor. Automatic temperature controls for the 25-
kilowatt electric heater maintained the desired compressor inlet temperature. A re-
motely operated pressure regulator was used to maintain compressor inlet pressure.
Compressor gas flow and exit pressure were regulated by an electrically operated butter-

9

Laboratory dry air supply

Isolation shutoff valve

Electric heater

Gas filter

Orifice

Isolation shutoff valves

Pressure control valve

Low pressure exhaust system and control valves

Turbine assembly

Turbine control valve

High pressure air supply
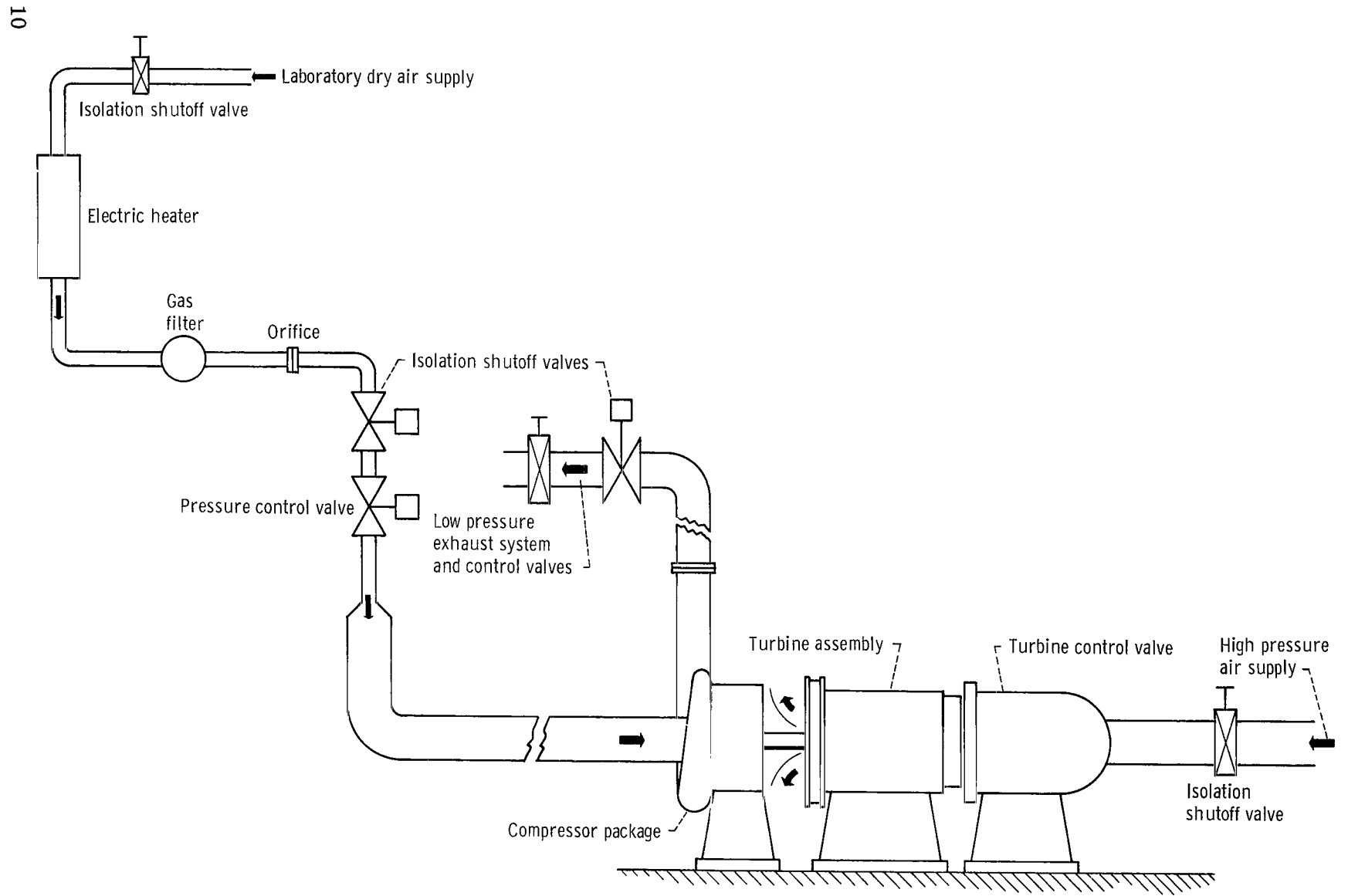
Isolation shutoff valve

Compressor package

CD-9755-01

Figure 5. - Compressor test facility.

fly valve and a remote pneumatic operated globe valve installed in parallel in the exhaust piping downstream of the research compressor. The globe valve was used as a vernier flow control valve to enable the facility operator to make small adjustments in compressor flow rate. The laboratory exhaust system carried the compressor gas flow to the atmosphere.

Laboratory dry air supply was also used as air supply source for the drive turbine. Airflow to the drive turbine was controlled by a modulated pneumatic valve. An automatic overspeed shutdown circuit was installed in the speed indicating system.

Instrumentation

Flow through the compressor was determined from a thin-plate orifice installed according to ASME standards in the compressor gas supply line (fig. 5). Overall compressor performance was computed from total pressures and total temperatures obtained at the compressor inlet and exit instrumentation stations 1 and 6 (fig. 3).

At station 1 the instrumentation consisted of three wall static-pressure taps equally spaced around the circumference and three combination total-pressure - temperature rakes. The total-pressure heads on the rakes were located radially at the centers of three equal annular areas and the spike iron-constantan thermocouples were placed midway between the total-pressure heads.

The compressor exit flow conditions (station 6, fig. 3) were measured with four wall static-pressure taps equally spaced around the circumference and four combination total-pressure - temperature rakes. The exit rakes were similar in design to the inlet-station combination total-pressure - temperature rakes.

The bearing lubricating oil inlet and outlet temperatures were measured by iron-constantan thermocouples. These temperatures were used in determining the heat loss to the lubricating oil.

Compressor static and total pressures were measured on a 100-inch (254-cm) mercury manometer board, recorded on film, and read to an accuracy of ±0.05 inch (0.13 cm) of mercury. All other data were measured by an automatic digital potentiometer and recorded on paper tape. The pressure drops across the thin plate orifice and orifice inlet pressure were measured with strain-gage transducers. The pressure ranges of these transducers were selected to maintain a pressure measuring accuracy within ±1.5 percent. Gas temperatures were measured by spike thermocouples with an estimated accuracy of $\pm1.5^{\circ}$ R (±0.8 K).

Compressor speed was indicated with the use of a magnetic pickup in conjunction with a gear mounted on the compressor shaft. In order to maintain constant compressor speed during test operations, an electronic control circuit was used with the pneu-

11

matic controls for regulating drive turbine airflow. This control circuit was capable of automatically maintaining compressor speed within ±1/2 percent of the speed set by the test facility operator.

Test Procedure

The compressor was operated over a range of weight flows from maximum flow to stall conditions at design speed for each of the following nominal inlet air pressures: 1.5, 1.9, 2.4, 3.0, 3.9, 6.0, and 8.6 psia (1.0, 1.3, 1.7, 2.1, 2.7, 4.1, and 5.9 N/m^2). Throughout the test series inlet temperature was maintained at nominal design conditions of 536$^\mathrm{o}$ R (297.8 K).

Calculation Procedure

The total-pressure ratio, temperature rise efficiency, and compressor work factor (overall performance stations 1 to 6, fig. 3) were calculated based on the equations defined in the symbol list. Measured pressures and temperatures were used for these calculations with the following exception:

As indicated in reference 4, in spite of all efforts to prevent heat transfer during compressor tests, two potential heat leak paths existed (1) heat transfer from the impeller outlet to the impeller inlet via the stationary aluminum shroud, and (2) heat loss to the compressor bearing oil supply. In this investigation an attempt was made to account for this heat flow out of the system to the bearing oil flow. No attempt was made to eliminate the heat flow back into the compressor inlet through the aluminum shroud. The heat loss from the compressor airflow to the oil flow was estimated based on the following procedure: First, the temperature rise in the oil due to bearing and seal friction was determined by evacuating the compressor to eliminate aerodynamic heating and then measuring the temperature rise of the oil at the speed at which the data were to be obtained. The temperature rise in the oil flow during actual testing was then measured, and the temperature rise due to bearing and seal friction subtracted. This difference in oil temperature rise is attributed to heat flow out of the gas passing through the compressor. The assumption is made that changes in aerodynamic thrust loading of the bearings has an insignificant effect on bearing friction. Pressure differences do not appreciably change the loading of the seal; thus, seal friction should be no different when testing the compressor evacuated or when testing at some inlet pressures. With the temperature rise in the oil flow being attributed primarily to the heat leak from the gas flow, a heat balance between the two fluids was made to determine the reduction in

compressor discharge gas temperature due to this heat leak. This temperature differ-
ence was added to the measured exit temperature to obtain a corrected exit temperature.
All performance data presented in the main body of this report were based on this cor-
rected exit temperature. The effects of this correction can be seen in appendix B where
the overall performance data at design speed and for the seven inlet pressure levels are
presented. There, the compressor efficiency and work factor are plotted based on both
the measured temperature rise and the corrected temperature rise which accounts for
the heat leak through the oil lubrication system.

The Reynolds number was calculated based on the total density at station 1 (fig. 3),
the impeller tip speed, the impeller tip diameter, and the dynamic viscosity at station 1.

RESULTS AND DISCUSSION

Comparison plots of total-pressure ratio and temperature rise efficiency at design
speed and for seven Reynolds numbers are presented in figures 6 and 7, respectively, as
a function of design equivalent weight flow. The values of inlet pressure corresponding to
each of the Reynolds numbers is presented in table III. All data were taken at a design
speed of 40 300 rpm and at a nominal design inlet temperature of 536° R (297.8 K).

As the Reynolds number was decreased from 1.8×10^6 to 0.32×10^6, both maximum
flow and surge points occur at progressively lower equivalent flow rates (figs. 6 and 7).
The maximum flow point dropped from approximately 115 to 106 percent of design equiva-
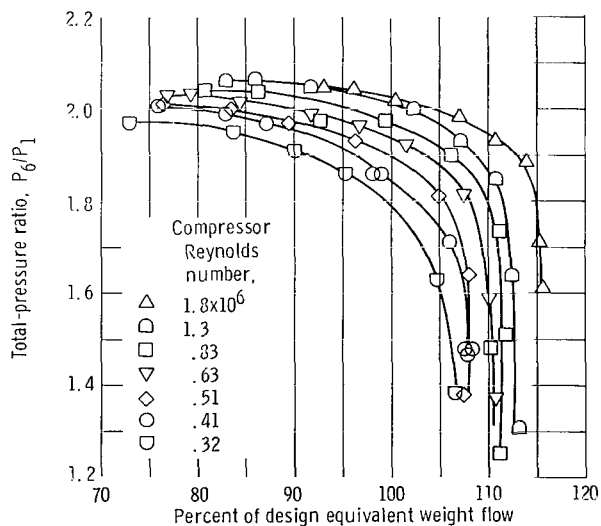lent weight flow while the surge point moved from an estimated 88 (surge was not es-

Figure 6. - Comparison of overall pressure ratio and flow
range at various Reynolds numbers for 6-inch
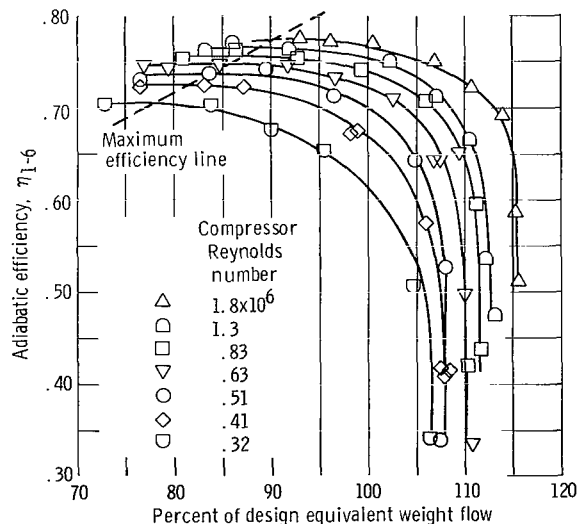(15.24-cm) centrifugal compressor at design speed.

Figure 7. - Comparison of overall efficiency and flow range
at various Reynolds numbers for 6-inch (15.24-cm)
centrifugal compressor at design speed.

TABLE III. - REYNOLDS

NUMBERS AND COR-

RESPONDING NOMINAL

INLET PRESSURES

Reynolds number, Re	Nominal inlet pressure	
	psia	kN/m^2
0.32×10^6	1.5	1.0
.41	1.9	1.3
.51	2.4	1.7
.63	3.0	2.1
.83	3.9	2.7
1.3	6.0	4.1
1.8	8.6	5.9

tablished at the highest Reynolds number) to approximately 73 percent of design equivalent weight flow as Reynolds number was decreased. Both maximum efficiency and maximum pressure ratio also occurred at lower equivalent weight flows with decreasing Reynolds number (figs. 6 and 7). Maximum efficiency and maximum pressure ratio dropped, respectively, from 0.775 to 0.706 and 2.05 to 1.97.

These trends can be explained in terms of the boundary-layer thickness increasing with lower Reynolds number, thereby decreasing the effective flow areas throughout the compressor. With the reduction in effective flow areas at lower Reynolds numbers, the compressor through-flow velocities (in the core flow) increase. This increase in through-flow velocity causes the flow angle at the impeller exit to decrease for a given equivalent flow. The maximum weight flow, the weight flow at maximum efficiency, and the surge flow rate are, at least in part, controlled by the flow angle leaving the impeller and those entering the vaned diffuser. Thus, the equivalent flow at which maximum flow, peak efficiency, and surge occur can be expected to vary with Reynolds number as is indicated by the data (figs. 6 and 7).

The compressor work factor f_{cw} is plotted against design equivalent weight flow in figure 8 for the seven Reynolds numbers at which the data were obtained. Interestingly, for this compressor, the work factor is a function of the equivalent weight flow only, rather than Reynolds number, since all the data fall on one line. Not all the data points are shown in figure 8 since for a given inlet pressure the work factor tends to change linearly with flow (appendix B).
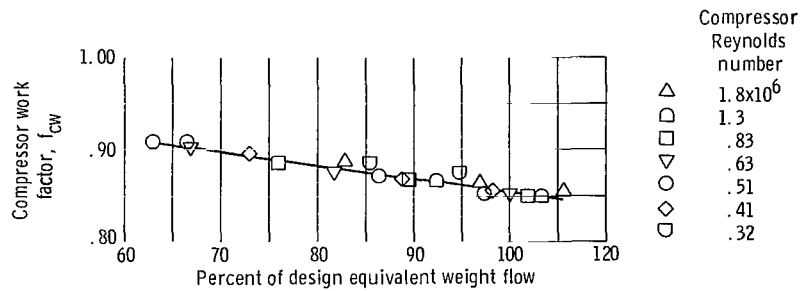
Figure 8. – Compressor work factor as function of percent of design equivalent weight flow for various Reynolds numbers.

The compressor work factor is defined as being equal to slip factor plus a windage factor (ref. 4) and is given by the following equation:

$$f_{cw} \equiv f_s + f_w = \frac{gJc_p\Delta T_{vd}}{U_{t3}^2} + \frac{gJc_p\Delta T_w}{U_{t3}^2} = \frac{gJc_p(\Delta T_{vd} + \Delta T_w)}{U_{t3}^2}$$

$$= \frac{gJc_p(T_6 - T_1)}{U_{t3}^2}$$

The slip factor is based on the gas temperature rise due to the energy addition associated with the vector diagrams, and the windage factor is based on the gas temperature rise due to the windage at the back face of the impeller and between the impeller vanes and stationary shroud. The compressor work factor is based on the measured temperature rise which includes both the temperature rise due to the vector diagram energy addition and the temperature rise due to windage.

In discussing the observed trend in compressor work factor with equivalent weight flow and Reynolds number, the slip factor will be considered as a function of equivalent flow rate and Reynolds number. If the relative flow angle leaving the impeller is assumed to be essentially constant (constant deviation), the slip factor will decrease linearly as through-flow velocity is increased. Thus, as equivalent flow rate is increased, slip factor should decrease. Since decreasing Reynolds number increases through flow velocity it should also decrease slip factor.

Windage factor f_w will be considered to be a function of weight flow and Reynolds number. Reference 5 indicates that the temperature rise due to windage ΔT_w, and

therefore f_w, decreases linearly as flow rate increases. In addition ΔT_w and thus f_w are shown to decrease with increasing Reynolds number proportional to the 0.2 power of Reynolds number for the flow regime encountered in this compressor.

In summary, both components of f_{cw}, f_s, and f_w should decrease with increasing equivalent weight flow as shown in figure 8. However, f_s should increase with increasing Reynolds number while f_w should decrease. Since all the work factor data for various Reynolds numbers fall on the same straight line (within data scatter), and the two components f_s and f_w that make up the work factor should show opposing trends with Reynolds number, it can be concluded that the Reynolds number effect on f_s for this compressor is approximately equal and opposite to that of f_w.

Figure 9 shows the efficiency at design weight flow and maximum efficiency plotted against percent of design Reynolds number. From 130 to 23 percent of design Reynolds number the efficiency at design equivalent weight flow dropped more than 15 points. The maximum efficiency also dropped with decreasing Reynolds number but less rapidly than
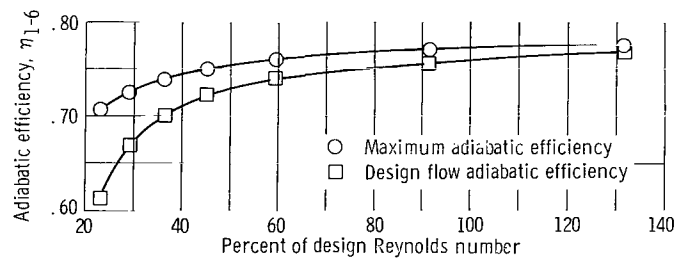

Figure 9. - Variation of maximum efficiency and design flow efficiency with Reynolds number for 6-inch (15.24-cm) centrifugal compressor at design speed. Design Reynolds number, 1.36×10^6.

the efficiency at design flow. Over the same range of Reynolds numbers, the maximum efficiency dropped only eight points or about half as much as that at design weight flow.

As stated earlier, when Reynolds number is reduced, the compressor through-flow velocities (in the core flow) increase. This causes off-design flow angles entering the vaned diffuser resulting in a rapid deterioration in pressure ratio and efficiency with decreasing Reynolds number at design equivalent weight flow. The peak efficiency drops with decreasing Reynolds number primarily because of viscous losses, whereas, for design weight flow, the efficiency decay is a result of both changes in viscous losses and off-design flow angles resulting in higher losses. The peak efficiency curve in figure 9

shows a more rapid decrease in efficiency at the lower Reynolds numbers, which suggests an exponential relation between Reynolds number and efficiency.

A relation between compressor efficiency η, or more specifically loss $(1 - \eta)$, and Reynolds number commonly used is

$$\frac{1 - \eta}{1 - \eta_{ref}} = \left(\frac{Re_{ref}}{Re}\right)^n$$

where η_{ref} and Re_{ref} are known values of efficiency and Reynolds number used as a reference point to predict η at other values of Re. The value of the exponent n generally used (ref. 6) in the Reynolds number range encountered here is 0.2. Figure 10 shows the loss $(1 - \eta_{max})$ against Reynolds number where the loss corresponds to the maximum efficiency points. A line for $n = 0.2$ is drawn through the measured loss at design Reynolds number for this compressor for comparative purposes. The 0.2 power relation seems to predict the losses with reasonable accuracy for Reynolds number below 1×10^6 since the slope of the two lines are approximately equal in this range. This indicates that the loss mechanism in this range of Reynolds number is primarily viscous friction associated with a turbulent boundary layer and an aerodynamically smooth surface. For Reynolds numbers below those encountered here, the losses might increase more rapidly than predicted by the 0.2 power due to a growing mismatch of the impeller and diffuser (i.e., the impeller peak efficiency and diffuser peak efficiency each occurring at different flow rates). Above 1×10^6 the change in loss with Reynolds number is much less than that predicted by the 0.2 power. This flattening of the curve might be attributed to the flow surfaces of this compressor being aerodynamically rough for Reynolds numbers somewhat above 1×10^6. This is analogous to flat plate Reynolds number data where an aerodynamically rough surface shows little or no change in losses with Reynolds number. This departure from the 0.2 power relation at Reynolds numbers above 1×10^6 has also been observed in the 3.2-inch (8.13-cm) centrifugal compressor of reference 7.
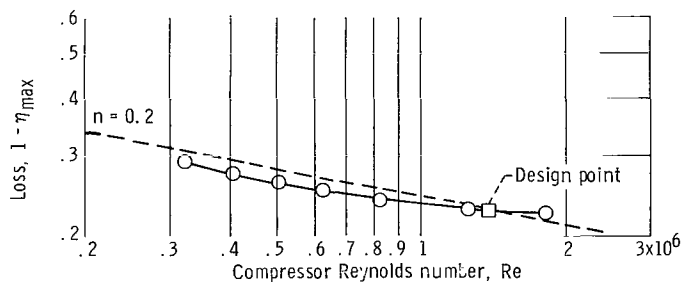

Figure 10. - Loss as function of Reynolds number for 6-inch (15.24-cm) centrifugal compressor at design speed.

CONCLUDING REMARKS

The 6-inch (15.24-cm) centrifugal compressor tested in air shows a progressive degradation in performance along with a lowering of the surge and maximum flow points with decreasing Reynolds number. This performance degradation can be explained by the changes in viscous losses and in effective flow areas due to boundary layer growth, which in turn causes changes in flow angles. The decrease in peak efficiency as Reynolds number is lowered is attributed primarily to increasing viscous losses. The more rapid drop in efficiency at design weight flow is attributed to both increasing viscous losses and to changing flow angles resulting in off-design operation of the diffuser vanes.

The compressor work factor f_{cw} decreased linearly with increasing equivalent weight flow, but the effect of Reynolds number was not noticeable.

The exponential (n = 0.2) relation commonly used between loss $(1 - \eta_{max})$ and Reynolds number seems to predict the losses associated with maximum efficiency with reasonable accuracy for Reynolds numbers below 1×10^6 on this compressor. For Reynolds numbers below 0.32×10^6 an impeller-diffuser mismatch may occur causing deviation from the 0.2 power relation. Above 1×10^6, a gradual leveling off of loss is attributed to the flow surfaces being aerodynamically rough.

Lewis Research Center,
    National Aeronautics and Space Administration,
        Cleveland, Ohio, January 23, 1970,
            120-27.

APPENDIX A

METHOD OF CORRELATION AND COMPARISON OF

AIR-ARGON OVERALL PERFORMANCE

The basic principle involved in correlating the performance of a centrifugal compressor from one gas to another is to establish geometric similarity between the vector diagrams of both gases at two locations. The locations used were the impeller inlet and the impeller exit. Because of differences in specific heat ratio, only two locations in the compressor can be matched with exact vector diagram similarity. Since iterations are involved in this procedure a computer program was written. The following is a summary of the operation of this program.

The gas in which the performance of the compressor is known will be designated A, and the gas in which the performance is being predicted will be designated B for the following discussion. The inlet flow coefficient φ and static density ratio across the impeller are calculated from the input of overall pressure ratio and efficiency, wheel speed, weight flow rate, and impeller efficiency at a particular operating point in gas A. Through an interactive process and assuming a constant slip factor, a compressor wheel speed is found for gas B that will match both inlet flow coefficient and density ratio across the impeller. Thus, the impeller velocity diagrams are made geometrically similar. In predicting the performance of gas B from that of gas A along a constant speed line, a slight variation in calculated speed for gas B will result over the weight flow range. In order to put the calculated performance for gas B on a constant speed line, a small (usually less than 1 percent) speed change is made. This is done by calculating a new temperature difference across the compressor by assuming that the temperature difference is proportional to the square of the wheel speed. From this a new total pressure and weight flow is found assuming the efficiency is constant over this small speed change. Reynolds number is matched by adjusting inlet pressure. No attempt is made to match Mach number. However, in the case of the correlation between argon and air almost all the Mach numbers match within 1 percent.

A comparison of the actual air performance to that predicted from argon data is shown in figure 11. The efficiency curves match exactly with respect to maximum efficiency and only differ by about 1.5 percent in flow at the maximum flow rate. The total pressure ratio for the predicted curve is slightly lower than the actual one (about 0.5

(a) Pressure ratio as function of percent of design equivalent weight flow.

(b) Efficiency as function of percent of design equivalent weight flow.
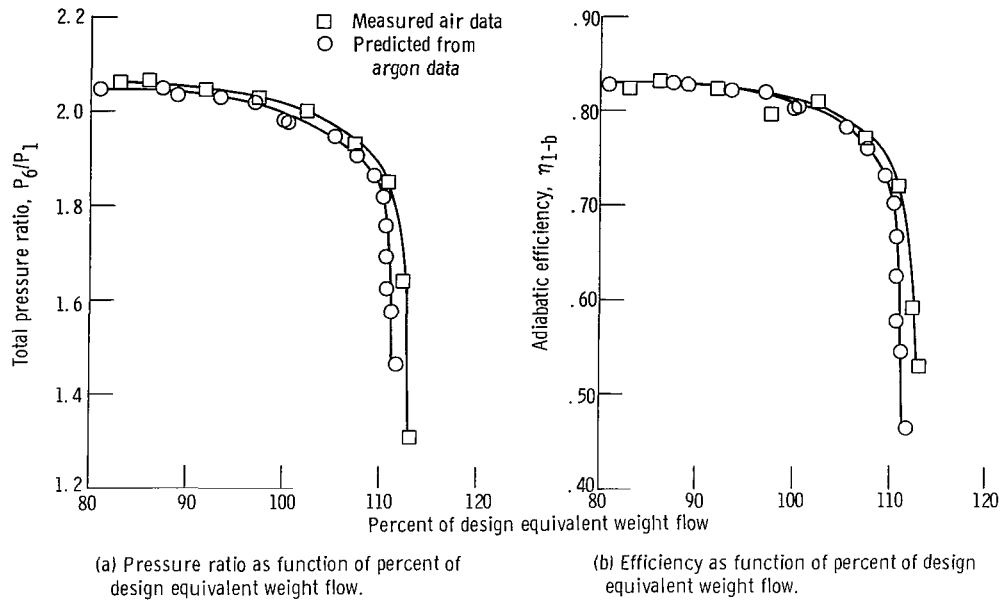
Figure 11. - Comparison of air performance with that predicted from argon data for 6-inch (15.24-cm) centrifugal compressor at design speed.

percent). These differences are in the order of data accuracy. These two sets of data were not taken at exactly the same Reynolds number. The air data Reynolds number is approximately 91 percent of the Reynolds number at which the argon data were obtained. However, this does not explain the slight differences in the two curves since it is in the wrong direction.

It is felt that this performance correlation technique is sufficiently accurate to permit testing of this compressor in air (although it was designed for argon as the working fluid) to determine the Reynolds number effect.

APPENDIX B

OVERALL PERFORMANCE

The overall pressure ratio, overall efficiency, and compressor work factor in air for the 6-inch (15.2-cm) radial bladed centrifugal compressor over a range of inlet pressure are presented in figure 12. The compressor was run at design speed (40 300 rpm for air) and design inlet temperature of 536° R (297.8 K). Both the as-measured and the corrected-for-heat-leak-to-oil efficiencies and compressor work factors are shown. This correction is applied to the measured temperature rise across the compressor, in order to account for the heat loss to the bearing oil supply. This heat loss is determined by a measured oil temperature rise, oil flow rate, and heat due to bearing and seal friction.
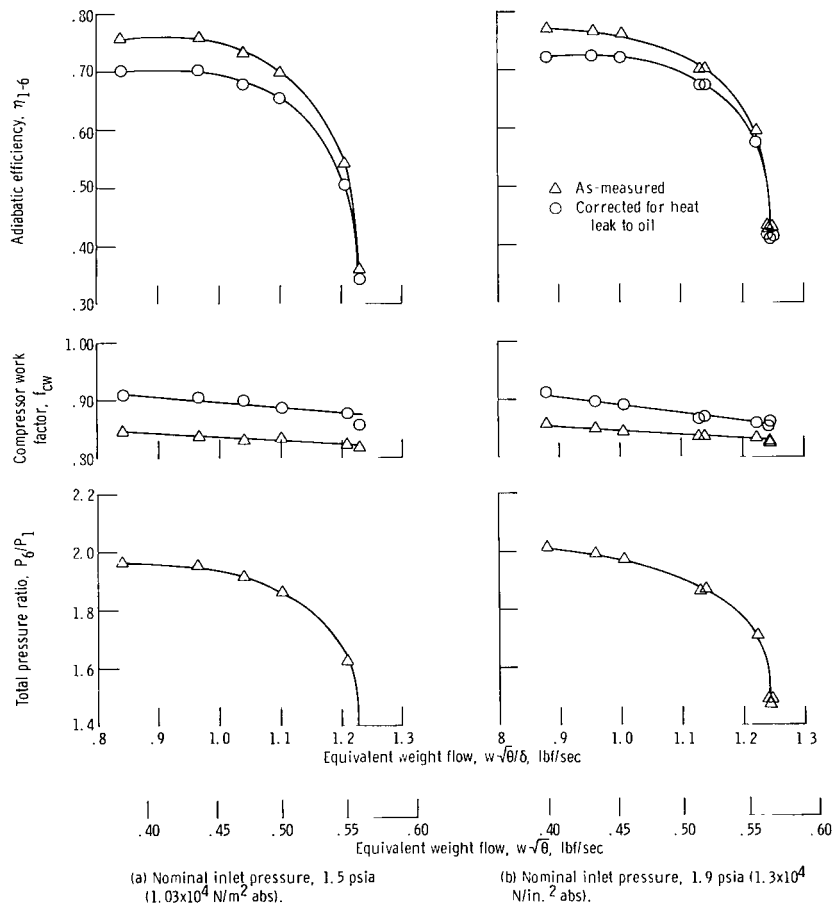

(a) Nominal inlet pressure, 1.5 psia (1.03x10⁴ N/m² abs).

(b) Nominal inlet pressure, 1.9 psia (1.3x10⁴ N/in.² abs).

Figure 12. - Overall performance at various inlet pressures for a 6-inch (15.24-cm) centrifugal compressor at design speed.
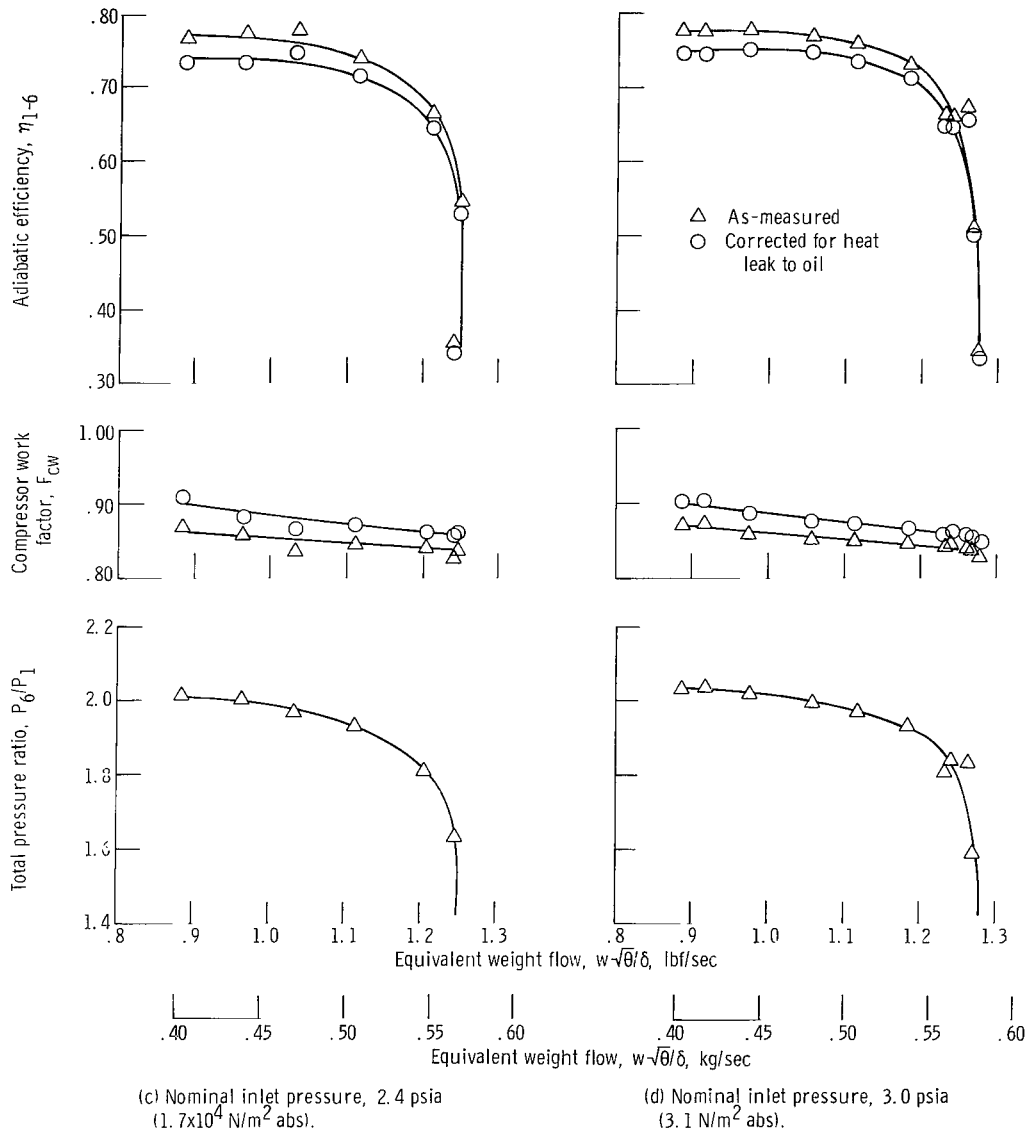
△ As-measured
○ Corrected for heat
   leak to oil

Equivalent weight flow, $w\sqrt{\theta}/\delta$, lbf/sec

Equivalent weight flow, $w\sqrt{\theta}/\delta$, kg/sec

(c) Nominal inlet pressure, 2.4 psia
(1.7x10^4 N/m^2 abs).

(d) Nominal inlet pressure, 3.0 psia
(3.1 N/m^2 abs).

Figure 12. - Continued.

(e) Nominal inlet pressure, 3.9 psia (2.7x10⁴ N/m² abs).

(f) Nominal inlet pressure, 6.0 psia (4.1x10⁴ N/m² abs).

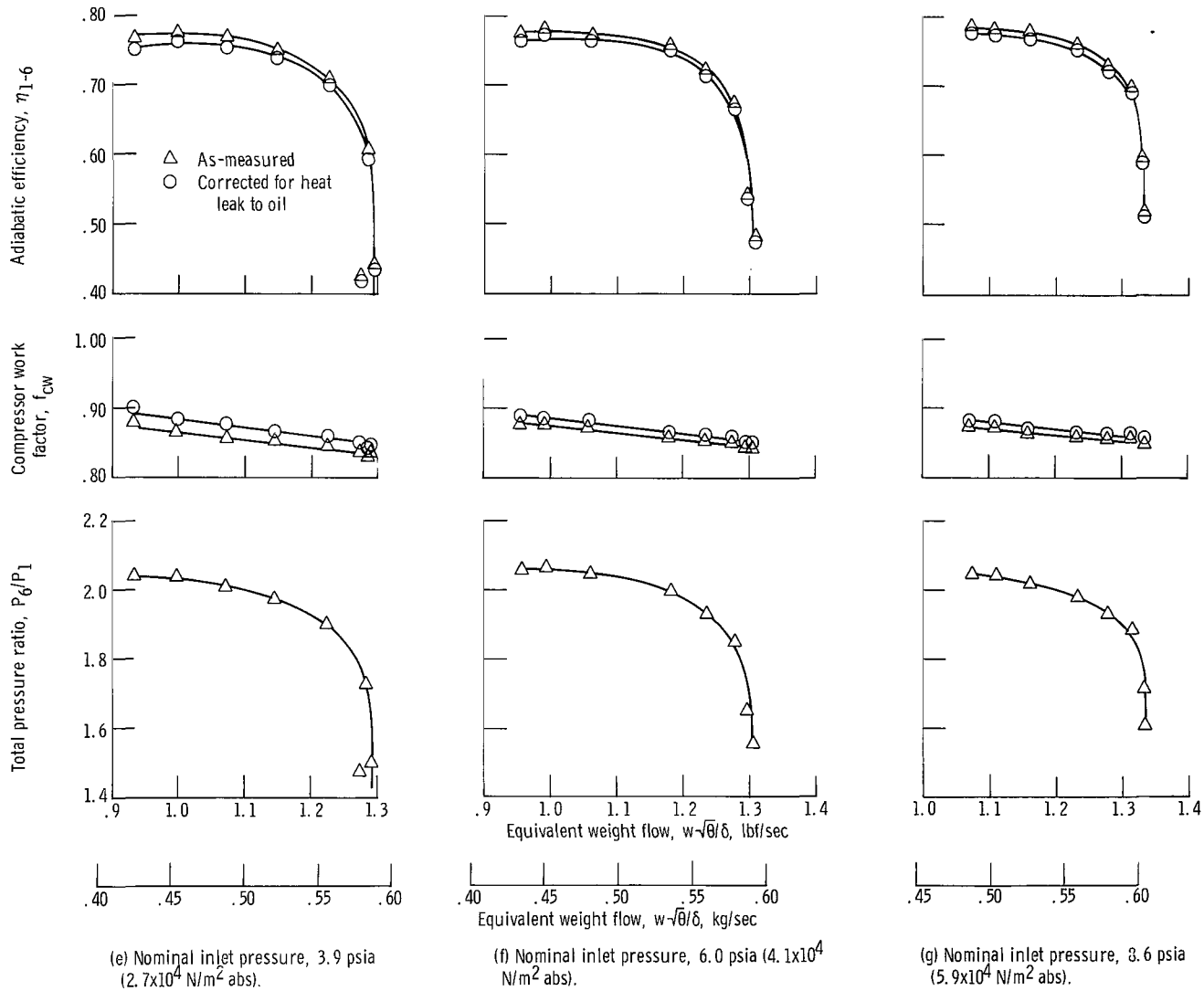(g) Nominal inlet pressure, 8.6 psia (5.9x10⁴ N/m² abs).

Figure 12. – Concluded.

REFERENCES

1. Stewart, Warner L.; Glassman, Arthur J.; and Krebs, Richard P.: The Brayton Cycle for Space Power. Paper 741A, SAE, Sept. 1963.

2. Harrack, W. G.; and Caldwell, R. T.: System Optimization of Brayton-Cycle Space Power Plants. Paper 63-WA-87, ASME, Nov. 1963.

3. Anon.: Design and Fabrication of a High-Performance Brayton-Cycle Compressor Research Package. Rep. APS-5109-R, AiResearch Mfg. Co. (NASA CR-54368), May 1968.

4. Tysl, Edward R.; Ball, Calvin L.; Weigel, Carl; and Heidelberg, Laurence J.: Overall Performance in Argon of a 6-inch Radial-Bladed Centrifugal Compressor. NASA TM X-1622, 1968.

5. Daily, J. W.; and Nece, R. E.: Chamber Dimension Effects on Induced Flow and Frictional Resistance of Enclosed Rotating Disks. J. Basic Eng., vol. 82, no. 1, Mar. 1960, pp. 217-232.

6. Bullock, R. O.: Analysis of Reynolds Number and Scale Effects on Performance of Turbomacninery. J. Eng. Power, vol. 86, no. 3, July 1964, pp. 247-256.

7. Perrone, G. L.; and Milligan, H. H.: Brayton Cycle 3.2-inch Radial Compressor Performance Evaluation. Rep. APS-5214-R, AiResearch Mfg. Co. (NASA CR-54968), May 1966.

*"The aeronautical and space activities of the United States shall be
conducted so as to contribute . . . to the expansion of human knowl-
edge of phenomena in the atmosphere and space. The Administration
shall provide for the widest practicable and appropriate dissemination
of information concerning its activities and the results thereof."*

— NATIONAL AERONAUTICS AND SPACE ACT OF 1958

NASA SCIENTIFIC AND TECHNICAL PUBLICATIONS

TECHNICAL REPORTS: Scientific and
technical information considered important,
complete, and a lasting contribution to existing
knowledge.

TECHNICAL NOTES: Information less broad
in scope but nevertheless of importance as a
contribution to existing knowledge.

TECHNICAL MEMORANDUMS:
Information receiving limited distribution
because of preliminary data, security classifica-
tion, or other reasons.

CONTRACTOR REPORTS: Scientific and
technical information generated under a NASA
contract or grant and considered an important
contribution to existing knowledge.

TECHNICAL TRANSLATIONS: Information
published in a foreign language considered
to merit NASA distribution in English.

SPECIAL PUBLICATIONS: Information
derived from or of value to NASA activities.
Publications include conference proceedings,
monographs, data compilations, handbooks,
sourcebooks, and special bibliographies.

TECHNOLOGY UTILIZATION
PUBLICATIONS: Information on technology
used by NASA that may be of particular
interest in commercial and other non-aerospace
applications. Publications include Tech Briefs,
Technology Utilization Reports and Notes,
and Technology Surveys.

Details on the availability of these publications may be obtained from:

SCIENTIFIC AND TECHNICAL INFORMATION DIVISION

NATIONAL AERONAUTICS AND SPACE ADMINISTRATION

Washington, D.C. 20546